JunB-HBZ nuclear translocation by TGF-β is a key driver in HTLV-1–mediated leukemogenesis

Wenyi Zhang[1], Takafumi Shichijo[1, *], Xueda Chen[1], Masao Matsuoka[1] and Jun-ichirou Yasunaga[1, *]

[1]Department of Hematology, Rheumatology and Infectious Diseases, Faculty of Life Sciences, Kumamoto University, Kumamoto, Japan

* Correspondence to Takafumi Shichijo, Jun-ichirou Yasunaga

Email: tshichijo@kumamoto-u.ac.jp, jyasunag@kumamoto-u.ac.jp

Competing Interest Statement: The authors declare no competing interests.

Keywords: HTLV-1, ATL, HBZ, JunB, TGF-β/Smad signaling pathway

This PDF file includes:

Main Text

Figure 1 to 6

Abstract

The *HTLV-1 bZIP factor* (*HBZ*) gene, which is the only viral gene conserved and consistently expressed in all adult T-cell leukemia-lymphoma (ATL) cases, is critical for ATL oncogenesis. Although HBZ protein is found in both the nucleus and the cytoplasm, the dynamics of HBZ protein localization and its contribution to oncogenesis have not been fully elucidated. In this study, we analyzed the subcellular expression pattern of HBZ in primary HTLV-1–infected T cells from asymptomatic carriers and leukemic cells of ATL patients using the Proximity Ligation Assay. Nuclear localization of HBZ protein was significantly higher in fresh ATL cells than in HTLV-1–infected cells from carriers. Importantly, translocation of HBZ protein from the cytoplasm to the nucleus after TGF-β activation was observed in ATL patients, but not in HTLV-1 carriers. In ATL cells, the cellular transcription factors JunB and pSmad3 interact with HBZ and facilitate its nuclear translocation upon TGF-β stimulation. *JUNB* knockdown inhibits cell proliferation *in vitro* and *in vivo* and promotes apoptosis in ATL cells but not in HTLV-1–infected non-leukemic cells, indicating that JunB has important roles in maintaining ATL cells. In conclusion, TGF-β-induced nuclear translocation of HBZ-JunB complexes is associated with ATL oncogenesis.

Introduction

The signaling induced by transforming growth factor β (TGF-β) has pleiotropic actions in a wide range of cellular processes, such as cell differentiation, proliferation, apoptosis, secretion of extracellular mediators, tissue fibrosis and epithelial-to-mesenchymal transition (EMT). When the TGF-β signaling pathway is activated, Smad3 protein is phosphorylated and forms a complex with Smad4, which then translocates to the nucleus to regulate the transcriptional activation of various genes[1]. The functions of TGF-β are dependent not only on cell type or cancer type but also on the particular stage of tumorigenesis. In the immune system, TGF-β exerts inhibitory effects in multiple ways[2]. TGF-β inhibits Th1 and Th2 differentiation, suppresses the trafficking and cytotoxic activities of CD8+ T cells and induces the differentiation of regulatory T cells (Tregs). Thus, activating the TGF-β signaling pathway enables cancer cells to evade host immunity. Notably, however, little is known about the role of TGF-β in T-cell malignancies.

Human T-cell leukemia virus type 1 (HTLV-1) is the first discovered human oncogenic retrovirus that primarily infects $CD4^+$ T cells[3, 4]. While most HTLV-1–infected individuals remain asymptomatic for life, HTLV-1 does induce a malignancy of $CD4^+$ T cells, named adult T-cell leukemia-lymphoma (ATL), in 2–5% of carriers after several decades of latency[5, 6]. Viral replication of HTLV-1 is typically suppressed *in vivo*, and persistent infection is established primarily through clonal proliferation of infected cells[7].

Among the HTLV-1 viral proteins, HTLV-1 basic leucine zipper factor (HBZ), which is encoded in the antisense strand of the provirus, is consistently expressed in all ATL cases[8, 9]. Knockdown of *HBZ* leads to suppression of ATL cell proliferation[7] and significantly reduces tumor formation and tissue infiltration by xenografts transplanted into immunocompetent mice[8, 10], indicating the potential necessity of *HBZ* in the oncogenesis of ATL. It is noteworthy that HBZ increases the number of induced Treg (iTreg) cells with high Foxp3 expression[11] by activating the TGF-β/Smad signaling pathway[12], which plays crucial roles not only in immunosuppression but also in promoting the proliferation of ATL cells[13]. Thus HBZ-mediated activation of the TGF-

β/Smad signaling pathway has a special impact on ATL leukemogenesis.

The HBZ protein has been reported to be localized in the nucleus when it is transiently overexpressed[12, 14]. We previously reported that subcellular localization of HBZ protein is changed by cell context, and HBZ protein can be localized in both nucleus and cytoplasm in T cells[15]. Indeed, it has been reported that HBZ protein tends to be present in both the cytoplasm and the nucleus in ATL cells, while it is expressed in the cytoplasm of infected cells from HTLV-1 carriers[16, 17]. HBZ contains three nuclear localization signals and a functional nuclear export signal sequence in its N-terminal region, indicating that it can be shuttled between the cytoplasm and the nucleus[18, 19]. HBZ interacts with various cellular factors, controlling their activities in both the nucleus and cytoplasm[15, 19]. However, it remains unclear how the subcellular localization of HBZ is regulated and what significance this may have in the oncogenesis of ATL.

In the present study, to evaluate intracellular localization of endogenous HBZ protein in fresh ATL/HTLV-1–infected cells, we employ a more precise and highly sensitive method, the proximity ligation assay (PLA). The results demonstrate that HBZ protein in fresh ATL cells exhibits a higher nuclear localization than in infected cells from carriers. Surprisingly, in response to TGF-β stimulation, HBZ protein translocates from the cytoplasm to the nucleus in ATL cells, but not in non-leukemic infected cells. Importantly, an AP-1 protein, JunB, which is a known binding partner of HBZ, was indispensable for its translocation to the nucleus and the exertion of the cell proliferation-promoting functions triggered by TGF-β stimulation. Notably, we also found that JunB is essential for ATL tumorigenesis *in vivo*. These results suggest that the link between the TGF-β/Smad pathway and translocation of the HBZ-JunB complex plays a master regulatory role in ATL oncogenesis.

Results

A higher fraction of HBZ is nuclear in ATL cells than in HTLV-1–infected cells.

We first analyzed the expression patterns of HBZ in ATL cell lines (MT1, ATL43T[+], ED, and TL-Om1), HTLV-1 immortalized cell lines (MT-4, and Hut102), and HTLV-1–infected cell lines derived from non-leukemic clones (ATL6, and ATL7)[20] using the Duolink® PLA. Fluorescence signals were objectively and quantitatively evaluated by ImageJ, and the proportion of nuclear signals in the total signal was calculated for each cell. Unlike transiently overexpressed HBZ, which is exclusively found in the nucleus[12, 15], HBZ in all the cell lines was distributed in both the nucleus and the cytoplasm, though the nuclear-cytoplasmic ratio varied (**Fig. 1a, b**, and Supplementary Fig. 1a). Compared to the ATL cell lines, HBZ exhibited a stronger tendency for cytoplasmic expression in the two HTLV-1–infected non-leukemic cell lines, indicating that the intracellular localization of HBZ differs between leukemic and non-leukemic cells. Notably, in the MT-1 cell line, approximately 60% of the HBZ protein signals are distributed in the nucleus. MT-1 has an equivalent viral gene expression profile to primary HTLV-1–infected cells[21, 22]. This led us to wonder whether the expression of HBZ in fresh ATL patient samples and HTLV-1–infected carrier samples might also differ in a similar way.

Therefore we examined HBZ expression in patient samples, including ten ATL patient samples（six acute-type, two smoldering-type, and two chronic-type), and six HTLV-1–infected carrier samples. In the ATL cases, the distribution of HBZ protein was throughout the cytoplasm and nucleus and the localization was usually higher in the nucleus (**Fig. 1c, left**, **Fig. 1d**, and Supplementary Fig. 1b, c). In contrast, in HTLV-1 carrier cells that expressed HBZ, more HBZ was found in the cytoplasm than in the nucleus (**Fig. 1c, right**, **Fig. 1e**, and Supplementary Fig. 1b, c). The proportion of nuclear localization of HBZ protein is significantly higher in fresh ATL cells compared to that of HTLV-1–infected cells from HTLV-1 carriers (**Fig. 1f**). Collectively, these data show that the nuclear localization of HBZ protein is associated with the disease status.

Activation of TGF-β induces translocation of HBZ protein from the cytoplasm to the nucleus.

In our previous studies, we demonstrated that signaling via the TGF-β/Smad pathway is enhanced by HBZ[12], a step which is critical for the oncogenesis of ATL[13]. Activation of TGF-β signaling induces the nuclear localization of phosphorylated Smad3 (pSmad3) protein[13, 23], which is a known binding partner of HBZ[12], suggesting that the activation of TGF-β may also change subcellular localization of HBZ.

To investigate whether TGF-β/Smad signaling indeed induces the nuclear translocation of HBZ, we stimulated ATL and HTLV-1–infected non-leukemic cell lines with recombinant TGF-β and observed the sub-localization of HBZ by Duolink® PLA. We found that in (leukemic) TL-Om1 cells, the nuclear proportion of HBZ protein was significantly increased after TGF-β stimulation (**Fig. 2a, b**). To confirm the accumulation of HBZ protein in the nucleus in response to TGF-β stimulation, we performed an immunoblot experiment, separating TL-Om1 cells into cytoplasmic and nuclear fractions. As shown in Supplementary Fig. 2a, the expression of HBZ protein was increased in the nucleus after TGF-β treatment. Furthermore, this shift in HBZ protein expression from the cytoplasm toward the nucleus was also observed in three other ATL cell lines (ED, Hut102 and ATL43T [+]) (**Fig. 2b** and Supplementary Fig. 2b). We next analyzed whether translocation of HBZ can also be induced by TGF-β in two non-leukemic HTLV-1–infected T-cell lines, ATL6 and ATL7. In clear contrast to its effect on ATL cell lines, TGF-β stimulation did not change the intracellular localization of the HBZ protein in either the ATL6 or ATL7 cell line; HBZ remained in the cytoplasm (**Fig. 2c, d** and Supplementary Fig. 2c).

Next we examined whether TGF-β-induced nuclear transportation of HBZ protein also occurred in fresh ATL or HTLV-1–infected cells obtained from patients or carriers respectively. In the majority of ATL patient samples, HBZ protein was translocated from the cytoplasm to the nucleus in response to TGF-β stimulation (**Fig. 2e-g**). In contrast, all HTLV-1 carrier samples showed no significant change in HBZ localization (**Fig. 2h-j**).

To investigate whether the altered localization of HBZ induced by TGF-β is due to

159 the influence of binding partners, we evaluated the binding of HBZ to pSmad3 by
160 Duolink® PLA. The PLA signal is only detectable when pSmad3 and HBZ proteins
161 interact with each other. As shown in Supplementary Fig. 3a-d, after activation of TGF-
162 β, the HBZ-pSmad3 complex was observed predominantly in the nucleus in the ATL
163 cell line TL-Om1 and in fresh ATL patient samples, whereas it remained in the
164 cytoplasm in the non-leukemic ATL7 cell line. These results suggest that the nuclear
165 localization of HBZ induced by TGF-β in ATL cells may occur via HBZ-Smad3
166 complexes being transported into the nucleus.
167 Collectively, our data indicate that HBZ protein shifts its localization from the
168 cytoplasm to the nucleus in response to TGF-β stimulation in ATL cell lines and fresh
169 ATL cells. However, this change in localization is not significantly observed in cell
170 lines derived from HTLV-1–infected non-leukemic clones or in the HTLV-1–infected
171 cells of carriers. These results indicate that the nuclear localization of HBZ protein
172 induced by TGF-β is associated specifically with ATL.
173
174 **Increased JunB facilitates the nuclear localization of HBZ in response to TGF-β**
175 **stimulation.**
176 To gain insight into the regulation of TGF-β stimulation in ATL cells, we performed
177 RNA-seq analysis on the ED cell line with or without TGF-β stimulation. Overall, 675
178 and 656 transcripts were differentially up- or down-regulated in ED cells after 2 h of
179 TGF-β stimulation compared to unstimulated cells (**Fig. 3a**). Consistent with our
180 previous studies[13], gene set enrichment analysis (GSEA) revealed that the TGF-β
181 signaling pathway affects a range of cell growth-related signaling pathways such as the
182 P53, E2F, apoptosis and G2M pathways, suggesting that the TGF-β signaling pathway
183 is important for ATL cell proliferation. Notably, the MYC-associated gene sets were the
184 most upregulated upon TGF-β stimulation (**Fig. 3b, c**). Despite the short duration of
185 TGF-β stimulation, the TGF-β pathway itself was also significantly upregulated. We
186 found that *JUNB* was one of the most upregulated genes (**Fig. 3d, e and g**). In contrast,
187 in the HTLV-1–infected non-leukemic ATL7 cell line, TGF-β stimulation has almost no
188 effect on gene expression level, and GSEA did not identify any significantly enriched

189 pathways（**Fig. 3f, g**）. This indicates that the ATL7 cell line is insensitive to TGF-β
190 stimulation. We next examined the expression of *JUNB* at the mRNA level in various
191 ATL cell lines with or without TGF-β treatment. After two hours of stimulation with
192 TGF-β, *JUNB* expression was increased in both ATL cell lines (ED and MT-1). In
193 contrast, in a non-leukemic HTLV-1–infected T-cell line (ATL7), TGF-β stimulation
194 slightly decreased *JUNB* expression (**Fig. 3h**). To further understand the mechanism
195 by which TGF-β stimulation increases *JUNB* expression, we performed ChIP-seq
196 analysis for pSmad3 after TGF-β activation. In the ATL cell lines ED and MT-1,
197 pSmad3 bound specifically to the *JUNB* promoter region, suggesting that pSmad3
198 directly promotes *JUNB* transcription. Thus ATL cell lines respond to TGF-β in the
199 expected manner: pSmad3 enters the nucleus and induces *JUNB* transcription.
200 Although pSmad3 has the ability to bind to the *JUNB* promoter region in non-leukemic
201 ATL7 cells, it does not appear to induce *JUNB* expression (Supplementary Fig. 4).
202 Recent studies have shown that like Smad3, JunB can shuttle between the cytoplasm
203 and the nucleus[24] and is a known binding partner of HBZ protein[25]. These facts suggest
204 that JunB may also play a role in the altered HBZ localization after TGF-β stimulation.
205 To validate this hypothesis, we first verified the binding of JunB and HBZ protein by
206 co-immunoprecipitation experiments (Supplementary Fig. 3a) and Duolink® PLA. In
207 the ATL cell line ED, the HBZ-JunB complex was predominantly expressed in the
208 nucleus. After stimulation with TGF-β, the nuclear localization of these complexes
209 increased further (**Fig. 4a, upper panel, Fig. 4b**). In the non-leukemic HTLV-1–
210 infected T-cell line ATL7, JunB-HBZ binding was also found mainly in the nucleus, but
211 we did not observe any significant change in localization after TGF-β treatment (**Fig.
212 4a, lower panel, Fig. 4b**). Furthermore, in two clinical samples from acute ATL cases,
213 translocation of JunB-HBZ complexes was also observed (**Fig. 4c, d**).
214 We further examined whether JunB and Smad3 are essential for the nuclear
215 translocation of HBZ. To this end, we knocked down the *JUNB* gene or the *SMAD3*
216 gene by short hairpin RNA (shRNA) in the ATL cell lines TL-Om1 and ED to observe
217 whether TGF-β stimulation could still induce translocation of HBZ protein. Compared
218 to the scramble shRNA–infected control group in which HBZ translocated to the

219 nucleus upon TGF-β stimulation as observed previously, the knockdown of either
220 *JUNB* or *SMAD3* prevented HBZ from moving to the nucleus in response to TGF-β
221 stimulation (**Fig. 4e, f**, and Supplementary Fig. 5a, b).
222 Taken together, these data demonstrate that the TGF-β-induced nuclear
223 translocation of HBZ depends on JunB and Smad3 forming complexes with HBZ and
224 thus facilitating its entry into the nucleus.
225
226 ***JUNB* knockdown promotes apoptosis in ATL cell lines.**
227 To further understand the function of JunB in ATL pathogenesis, we transduced
228 lentivirus vectors expressing shRNA against *JUNB* into ED cells, MT-1 cells, and the
229 two non-leukemic HTLV-1–infected cell lines ATL6 and ATL7 (Supplementary Fig.
230 6a, b). We performed a cell proliferation assay to observe the effect of *JUNB*
231 suppression on ATL cell proliferation. In the ED and MT-1 cell lines, *JUNB* inhibition
232 significantly inhibited ATL cell proliferation (**Fig. 5a**). In contrast, inhibition of *JUNB*
233 in the two non-leukemic clone cell lines did not affect their cell growth, suggesting
234 that proliferation of these non-leukemic cell lines was not dependent on *JUNB* (**Fig.**
235 **5b**).
236 To further understand the mechanism by which *JUNB* suppression inhibited the
237 growth of ATL cell lines, we performed RNA-seq in two ATL cell lines (ED and MT-
238 1) and a non-leukemic HTLV-1-infected cell line (ATL7), each transduced with
239 shJUNB or scramble shRNA. Notably, the apoptosis related gene set was significantly
240 upregulated in both the ED and MT-1 cell lines (**Fig. 5c, d**, and Supplementary Fig.
241 6c). In contrast, the apoptosis-related gene set was not significantly altered in the
242 ATL7 cell line (**Fig. 5e**). Moreover, we identified 2054 genes whose expression was
243 significantly changed in the ED and MT-1 cell lines, but not in the ATL7 cell line
244 (**Fig. 5f**). KEGG analysis also revealed that these genes were mainly associated with
245 the cell cycle and apoptosis (**Fig. 5g**). These results were consistent with the results of
246 the proliferation experiments, where suppression of *JUNB* expression affected the
247 ATL cell lines but not the non-leukemic cells. Thus *JUNB* has leukemic cell-specific
248 functions critical for the persistence of ATL cells.

To elucidate the potential mechanisms of JunB-dependent transcriptional regulation in ATL cell lines vs. the HTLV-1–infected non-leukemic cell line, we performed ChIP-seq analysis for JunB in ED, MT-1 and ATL7 cells infected with shJUNB or scramble shRNA. To focus on genes directly regulated by JunB, we looked for genes that had JunB ChIP-seq peaks and were differentially expressed (upregulated or downregulated) by knockdown of *JUNB* (**Fig. 5h**). Thus we defined a set of 63 genes directly regulated by JunB specifically in both ED and MT-1 cells. *BCL2L11*, which is a pro-apoptotic BCL family gene, was one of the most enriched genes in the apoptosis gene set in the ED and MT-1 cell lines in our RNA-seq data. *JUNB* knockdown induced expression of *BCL2L11*, suggesting that this upregulation led to apoptosis in ATL cells (Supplementary Fig. 7, left). Additionally, *JUNB* regulated a set of regulatory T cell-related genes, such as *IL2RA*, *IL2RB*, and *SOCS2*, in ATL cell lines (**Fig. 5f**). Moreover, *JUNB* directly promoted the expression of *IL2RA* in ATL cell lines (Supplementary Fig. 7, right). In contrast, in the non-leukemic cell line, the expression level of *BCL2L11* is not regulated by JunB, which might explain why the proliferation of non-leukemic cells is not affected by the loss of *JUNB*. Thus the development of ATL appears to involve JunB becoming a regulator of genes that it previously did not regulate in HTLV-1 carrier cells.

We also evaluated the role of *JUNB* in the TGF-β signaling pathway of ATL cells. We knocked down *JUNB* in ED cells and performed RNA-seq before and after TGF-β stimulation (**Fig. 5i, left**). Compared to parental ED cells (**Fig. 3e**), the number of differentially expressed genes under TGF-β stimulation was significantly reduced when *JUNB* was knocked down, and those genes that were up-regulated, such as *SKIL*, *SMAD7*, and *BMF*, were known negative regulators of the TGF-β/Smad signaling pathway[26, 27]. Furthermore, GSEA showed that only the TGF-β signaling pathway was significantly upregulated when *JUNB* was knocked down. In contrast, pathways enriched by TGF-β stimulation in parental ED cells (**Fig. 3b**), such as cell growth-related signaling pathways and the MYC pathway, were not significantly enriched when *JUNB* was knocked down (**Fig. 5i, right**). Similar results were also observed in the MT-1 cell line (Supplementary Fig. 8a, b). These results demonstrate that *JUNB* is an

important activator of the TGF-β signaling pathway in ATL cells.

Collectively, through a combined analysis of RNA-seq and ChIP-seq, we defined the set of genes directly regulated by JunB in ATL cells and demonstrated that JunB is an important activator of the TGF-β signaling pathway in ATL cells. We also found that JunB activates gene sets associated with cell proliferation and inhibits the expression of the pro-apoptotic gene *BCL2L11*. Importantly, only in ATL cells, but not in non-leukemic infected cells, does JunB serve as a core regulator. Thus JunB plays a distinct and critical role in the oncogenesis of ATL.

JUNB is critical for ATL cell growth _in vivo_

A previous study has shown that knockdown of *HBZ* gene expression significantly reduces the size and infiltration of ATL tumors *in vivo*[10]. Given the core regulatory role of the JunB-HBZ axis in ATL oncogenesis, we were interested in testing the regulatory function of JunB in an *in vivo* environment. To this end, we knocked down the *JUNB* gene in two ATL cell lines, MT-1 and ED, and injected these cells subcutaneously into NOD/SCID/γ-chain knockout (NSG) mice to observe the growth of tumor cells (**Fig. 6a**). In both cell lines, all five mice in the control groups without *JUNB* knockdown successfully developed tumors. However, in the shJUNB-MT-1 injected group, we did not observe tumor formation in any of the five mice (**Fig. 6b-d**). In the shJUNB-ED injected group, *JUNB* knockdown significantly inhibited tumor size and tumor growth compared to the control mice (**Fig. 6e-g**). These results suggest that JunB plays an indispensable role in ATL tumorigenesis *in vivo*.

309 **Discussion**

310 *HBZ*, which is a central viral gene in HTLV-1 pathogenesis, is consistently expressed
311 not only in ATL cells but also in infected cells from HTLV-1 carriers; however, the
312 functional differences of HBZ in these different contexts remain unclear. Elucidating
313 the mechanisms underlying these differences is crucial for understanding ATL
314 oncogenesis. In this study, we found that nuclear localization of HBZ protein is higher
315 in ATL cells than in non-leukemic HTLV-1–infected cells. Furthermore, TGF-β
316 activation causes HBZ protein translocation from the cytoplasm into the nucleus only
317 in ATL cells but not in non-leukemic infected cells, suggesting that TGF-β-induced
318 nuclear localization of HBZ is associated with ATL oncogenesis. It remains unclear
319 why HTLV-1–infected cells that are not leukemic fail to respond to TGF-β in a similar
320 manner. Discovering the "trigger" that converts an infected cell from TGF-β
321 nonresponsive to responsive is an important issue that needs to be clarified in the future.

322 It is known that HBZ is involved in the regulation of multiple oncogenic pathways
323 by interacting with many transcription factors and transcription co-activators, such as
324 Smad proteins, CBP/p300[12, 13], and the AP-1 proteins[25, 28, 29]. Additionally, HBZ also
325 regulates the activity of transcription factors. For example, HBZ drives the expression
326 of BATF3 in ATL cells, regulating the BATF3/IRF4 transcriptional network[30]. These
327 findings support the crucial functional role of nuclear HBZ in ATL oncogenesis. In
328 particular, co-localization of JunB with HBZ in the nucleus is thought to be critical for
329 ATL development, as shown in this study.

330 Previous research has reported that JunB is expressed in all ATL cases and that the
331 loss of *JUNB* is toxic to ATL cell lines[31]. However, the mechanism of JunB regulation
332 in ATL remains unclear. We demonstrate here that TGF-β upregulates the expression of
333 *JUNB* and induces JunB-HBZ complex translocation to the nucleus in ATL cells but
334 not in non-leukemic cell lines. Additionally, the cytotoxicity resulting from the
335 knockdown of *JUNB* is only present in ATL cell lines, while non-leukemic cell lines
336 continue to proliferate normally in the absence of *JUNB*, indicating that *JUNB* is a
337 master transcription factor for oncogenic properties of ATL cells. JunB has been
338 reported to play a crucial role in the proliferation of helper T cell subsets by inhibiting

339 the expression of the pro-apoptotic gene *BCL2L11* (encoding Bim)[32]. In this study, we
340 found that JunB suppresses Bim expression by binding directly to the *BCL2L11*
341 genomic region, thereby protecting ATL cells from apoptosis. However, in the non-
342 leukemic HTLV-1–infected cell line, this regulatory function of JunB was absent and
343 *JUNB* deficiency did not have cytotoxic effects.

344 ATL cells have immunophenotypes that closely resemble that of iTreg cells, due to
345 the induction of the *FOXP3* gene by HBZ[33]. It is well known that naïve T cells
346 differentiate into iTregs by inducing Foxp3 through TGF-β stimulation[34]. Previously,
347 we reported that HBZ-Tg mice have an increased number of iTregs with high Foxp3
348 expression and develop inflammation and T-lymphomas[11]. Those findings suggest that
349 expansion of Tregs triggered by HBZ accelerates oncogenesis in this subset. Notably,
350 JunB has been reported to promote the expression of Treg effector molecules[35] and Treg
351 differentiation through the IL-2 pathway[36]. Our RNA-seq and ChIP-seq data suggest
352 that JunB directly upregulates *IL2RA* expression to increase sensitivity to IL-2, thereby
353 promoting the formation of the Treg phenotype in ATL cells. Previous studies showed
354 that like JunB, HBZ targets these genes, *BCL2L11*[37] and *IL2RA*[30]. Indeed, it has been
355 shown that HBZ suppresses transcription of *BCL2L11* in the nucleus[37]. It is noteworthy
356 that super-enhancers are present at the *IL2RA* locus in ATL cells[30], suggesting that the
357 JunB and HBZ proteins are recruited to the locus and coordinately regulate the
358 transcription of multiple genes during ATL oncogenesis.

359 Interestingly, recent study has shown that, in breast cancer cells, *JUNB* is a late-
360 responding gene induced by TGF-β stimulation and creates a feed-forward regulatory
361 network that enhances their invasive capacity[38, 39]. Here we show that activation of the
362 TGF-β signaling pathway causes pSmad3 to be recruited to the *JUNB* promoter region,
363 where it directly stimulates *JUNB* expression in ATL cells, but not in non-leukemic
364 HTLV-1–infected cells. Meanwhile, pSmad3 and JunB also facilitate the nuclear
365 translocation of HBZ, where it exerts its oncogenic functions; our findings suggest that
366 HBZ expands leukemic cells by reinforcing the link between TGF-β signaling and
367 *JUNB*-induced cell proliferation, which, as we have shown, becomes critical for the
368 survival of ATL cells.

369 Besides HTLV-1, other human oncogenic retroviruses also encode proteins that
370 promote infection and oncogenic processes through various mechanisms in the nucleus.
371 In human papillomavirus (HPV), the E6 and E7 proteins interfere with cell cycle
372 regulation by affecting nuclear proteins such as the tumor protein p53 (TP53) and
373 retinoblastoma (Rb)[40]. In Epstein–Barr virus (EBV), Epstein–Barr nuclear antigen 1
374 (EBNA-1) helps maintain viral DNA in the nucleus and regulates viral gene expression,
375 while the latent membrane protein 1 (LMP1) acts in the nucleus to promote cell
376 proliferation[41]. In addition, the nuclear localization of the hepatitis B virus (HBV)-
377 encoded oncogene X protein (HBx) is essential for promoting HBV replication, thereby
378 contributing to the development of hepatocellular carcinoma (HCC)[42, 43, 44]. The
379 subcellular localization of HBx may be influenced by its abundance [45] and interactions
380 with cellular proteins[46, 47]. However, there is no clear consensus on the preferential
381 subcellular localization of these viral proteins in viral oncogenesis. Our results confirm
382 that viral proteins may achieve nuclear translocation under signaling pathway
383 stimulation with the help of binding proteins. Identification of suitable binding proteins
384 could provide insight into the subcellular translocation mechanisms of other viral
385 proteins.
386 In conclusion, our study demonstrates that the nuclear localization of HBZ protein
387 is associated with disease status, and is likely influenced by differences in
388 responsiveness to TGF-β. Upon TGF-β stimulation, cytoplasmic HBZ can bind with
389 pSmad3 or JunB and translocate into the nucleus in ATL cells (Supplemental Fig. 9).
390 Having entered the nucleus, HBZ can further act to upregulate the TGF-β pathway,
391 creating a sort of positive feedback loop that maintains this pathway in an activated
392 state. In addition, HBZ and JunB act to upregulate other genes associated with
393 proliferation and the Treg phenotype. The result would be leukemic cells that are
394 constantly driven to proliferate — a crucial step in oncogenesis. This discovery of the
395 Smad3-JunB-HBZ cascade induced by TGF-β could pave the way for development of
396 therapeutic strategies against this fatal malignancy.
397

398 **Methods**

399 **Clinical samples**

400 All patients were fully informed about the purpose and procedures of this study.
401 Written informed consent was obtained in accordance with the Declaration of
402 Helsinki and received approval from the Institutional Review Board of Kumamoto
403 University (Genome 297). Peripheral blood mononuclear cells (PBMCs) were isolated
404 from patients with adult T-cell leukemia-lymphoma (ATL) and human T-cell leukemia
405 virus type 1 (HTLV-1) carriers by Ficoll-Paque PLUS (GE Healthcare).

406

407 **Cell lines**

408 Human embryonic kidney cell lines HEK293T purchased from American Type
409 Culture Collection were cultured in Dulbecco's modified Eagle's medium (Nacalai
410 Tesque) supplemented with 10% fetal bovine serum (FBS) and antibiotics. HTLV-1
411 immortalized cell lines (MT-2, MT-4 and Hut102) and ATL cell lines (MT-1, ED, TL-
412 Om1, ATL43T[+]) were cultured in RPMI 1640 (Nacalai Tesque) with 10% FBS and
413 antibiotics. HTLV-1–infected non-leukemia cell lines (ATL6, ATL7) and an ATL cell
414 line (ATL55T [+]) were cultured in RPMI 1640 (Nacalai Tesque) with 10% FBS,
415 recombinant human IL-2 and antibiotics.[8]

416

417 **Mice**

418 NOD.Cg-PrkdcscidIl2rgtm1Wjl /SzJ (NSG) mice were purchased from Charles River
419 Laboratories Japan, Inc. All animal experiments were performed in accordance with
420 Kumamoto University Animal Care and Use Committee guidelines and were
421 approved by the Committee.

422

423 **Duolink® Proximity Ligation Assays**

424 Cell lines or PBMCs extracted from patient blood samples were incubated with or
425 without recombinant human TGF-β1 (Wako, 20ng/ml) for 1 hour at 37°C. Cells were
426 washed twice with Dulbecco's Phosphate-Buffered Saline (D-PBS) and adjusted to the
427 appropriate cell number, then concentrated onto glass coverslips (Matsunami Glass)

428 by Cytospin (Shandon). Cells were then fixed in 4% paraformaldehyde for 15 minutes
429 at room temperature, permeabilized with 0.2% Triton X-100 for 15 minutes at room
430 temperature, and blocked with Duolink® Blocking Solution for 30 minutes in 37°C,
431 then stained with mouse anti-HBZ antibody (1A10, generated by immunizing
432 C57BL/6 mice with keyhole limpet hemocyanin [KLH]- conjugated HBZ peptide 97-
433 133 [CKQIAEYLKRKEEEKARRRRRAEKKAADVARRKQEEQE]) and either
434 rabbit anti-HBZ polyclonal antibody, generated by immunizing with HBZ-peptides
435 (CRGPPGEKAPPRGETH and QERRERKWRQGAEKC) (Medical & Biological
436 Laboratories) or JUNB Rabbit mAb (3753, Cell Signaling) or Phospho-SMAD3
437 (C25A9) Rabbit mAb (Cell Signaling) diluted in Duolink® Antibody Diluent (1x)
438 overnight at 4°C. Then, cells were incubated with Duolink® In Situ PLA® Probe
439 Anti-Mouse PLUS and Duolink® In Situ PLA® Probe Anti-Rabbit MINUS in 37 °C
440 for 1 hour, then incubated with Duolink® 5x Ligation Buffer and Duolink®
441 Polymerase (10U/µl) at 37°C for 30 minutes, and finally incubated with Duolink®
442 Amplification Red (5x) and Duolink Ligase (1 U/µl) at 37 °C for 100 minutes. The
443 glass coverslips were sealed with Duolink ® In Situ Mounting Medium with DAPI.
444 The cells were observed with a C2 confocal microscope (Nikon) and analyzed with
445 ImageJ. Data was collected from 20 randomly selected HBZ-expressing cells for
446 each sample.
447
448 **Co-immunoprecipitation experiments**
449 For endogenous immunoprecipitation experiments, MT-2 and ATL55T (+) cells were
450 lysed in RIPA lysis buffer with protease inhibitor for 30 min on ice. Rabbit anti-HBZ
451 polyclonal antibody (Medical & Biological Laboratories) was used for
452 immunoprecipitation. Normal rabbit IgG (Wako) was used as a control. The lysates
453 were immunoprecipitated with antibody conjugated Dynabeads™ Protein G Magnetic
454 Beads (Invitrogen).
455
456 **Extraction of cytoplasmic and nuclear proteins**
457 TL-Om1 cells were treated with or without recombinant human TGF-β1 (Wako,

488 7178bhf), *SMAD3*(VB900050-5901tdd, VB900050-5907vsa) and the negative control
489 were purchased from Vector Builder. Lentiviral vectors were generated by transient
490 transfection of HEK293T cells. The lentiviral vectors were harvested 48 hours after
491 transfection and used immediately for infection. After 24 hours of infection, target
492 cells were transferred into fresh growth medium, and the stably transfected cells were
493 selected in puromycin.
494
495 **RNA extraction and Quantitative RT-PCR**
496 Total RNA was extracted using the ReliaPrep RNA Miniprep System (Promega)
497 following the manufacturer's instructions. 1 μg of total RNA was synthesized into
498 cDNA with Superscript IV Reverse Transcriptase (Thermo Fisher Scientific).
499 Semiquantitative RT-PCR was performed using FastStart Universal SYBR Green
500 Master (Roche) and the StepOnePlus Real-Time PCR System (Applied Biosystems).
501 The primers used were as follows: JUNB-forward 5'-
502 CGATCTGCACAAGATGAACCACG-3', JUNB-reverse 5'-
503 CTGCTGAGGTTGGTGTAAACGG-3'.
504
505 **Cell proliferation assay**
506 After knockdown of *JUNB* and selection in puromycin, cells were plated at an
507 appropriate cell density in 96-well plates. The Cell Counting Kit-8 (DOJINDO
508 LABORATORIES) was used according to the manufacturer's instructions to assess
509 the proliferation of cells.
510
511 **RNA-sequencing**
512 For RNA sequencing, each experiment contained 3 biological replicates. RNA
513 samples were extracted using the ReliaPrep RNA Miniprep System (Promega). Total
514 RNA was provided for library preparation and sequencing to Macrogen, which used
515 the TruSeq Stranded mRNA Library Prep Kit and NovaSeq6000 (Illumina). After
516 cleaning the row reads with Trimmomatic[48], reads were mapped to hg38 by STAR.
517 Differential gene expression was analyzed by RSEM[49] and edgeR[50]. Differentially

518 expressed genes (log2 Fold change < -0.5 or > 0.5, FDR< 0.05) were further analyzed
519 using Gene Set Enrichment Analysis by GSEA software[51] or KEGG (Kyoto
520 Encyclopedia of Genes and Genomes) enrichment analysis[52].
521
522 **ChIP-sequencing**
523 After cells were treated with or without TGF-β for 2 hours, cells were collected and
524 ChIP DNAs were prepared using the SimpleChIP Enzymatic Chromatin IP Kit (Cell
525 Signaling Technology) according to the manufacturer's instructions. For Chromatin IP,
526 JunB Rabbit mAb (Cell Signaling Technology) or Phospho-SMAD3 (C25A9) Rabbit
527 mAb (Cell Signaling Technology) was used. DNA sequencing libraries were
528 generated on the Illumina NovaSeq6000 platform using the TruSeq ChIP Library
529 Preparation Kit (Illumina) with a standard 150-bp paired-end read protocol. Fastq files
530 were trimmed and qualified with Trimmomatic and Fastqc. Trimmed reads were
531 mapped using Bowtie2 aligned to the human genome (hg19)[53]. Reads that aligned
532 twice or more and unassembled reads (chrM, random and chrUn) were removed by
533 using samtools[54]. PCR duplicates were also deleted with Picard (MarkDuplicates).
534 Subsequently, by using samtools with the "-q 30" option, we selected reads with a
535 mapping quality of more than 30. The ENCODE Blacklist genome regions were also
536 deleted by using BEDtools[55]. ChIP-seq peaks were assessed by MACS2[56] with the "-p
537 1e-5" option using the corresponding input-sequenced file as a control. Extracted
538 peaks were then annotated to the nearest genes of the hg19 by using ChIPseeker[57]. To
539 visualize deep-sequencing data, we used samtools, deeptools[58] and SparK
540 (https://github.com/harbourlab/SparK).
541
542 **Xenograft experiments**
543 ED and MT-1 cell lines were infected with Scramble shRNA or shJUNB lentivirus,
544 followed by puromycin selection. Two million cells for each cell line were injected
545 subcutaneously into 6-week-old female NSG mice. When the tumor size became
546 approximately 50 mm^3, the subcutaneous tumor burden was measured every two days
547 using calipers. Tumor volumes (mm^3) were calculated using the following formula:

548 0.5 x (longest length) x $(width)^2$. On day 14 after the beginning of measurement, the
549 mice were sacrificed, and tumor weight was measured. In general, animals were
550 sacrificed when their tumors reached 2cm or when the mice became moribund.
551
552 **Statistical analysis and data visualization**
553 All data was statistically analyzed using the two-tailed unpaired Student's t test using
554 Prism 10 (GraphPad Software). All experiments were performed with at least three
555 biological replicates. The minimum significance level was set at $P < 0.05$. Asterisks
556 indicate the statistical significance as follows: *$P < 0.05$; **$P < 0.01$; ***$P < 0.001$;
557 **** $P < 0.0001$. Schematic diagrams in this study were created with BioRender.com.
558
559 **Data and materials availability:**
560 Data of deep sequence, RNA-seq, and ChIP-seq in this study will be deposited at the
561 DDBJ database and be publicly available as of the date of publication.
562

563 **References**

564 1. Heldin CH, Miyazono K, ten Dijke P. TGF-beta signalling from cell membrane
565 to nucleus through SMAD proteins. *Nature* **390**, 465-471 (1997).
566
567 2. Aftabi S*, et al.* Therapeutic targeting of TGF-beta in lung cancer. *FEBS J*,
568 (2024).
569
570 3. Proietti FA, Carneiro-Proietti AB, Catalan-Soares BC, Murphy EL. Global
571 epidemiology of HTLV-I infection and associated diseases. *Oncogene* **24**, 6058-
572 6068 (2005).
573
574 4. Poiesz BJ, Ruscetti FW, Gazdar AF, Bunn PA, Minna JD, Gallo RC. Detection
575 and isolation of type C retrovirus particles from fresh and cultured lymphocytes
576 of a patient with cutaneous T-cell lymphoma. *Proc Natl Acad Sci U S A* **77**,
577 7415-7419 (1980).
578
579 5. Matsuoka M, Jeang KT. Human T-cell leukaemia virus type 1 (HTLV-1)
580 infectivity and cellular transformation. *Nat Rev Cancer* **7**, 270-280 (2007).
581
582 6. Ishitsuka K, Tamura K. Human T-cell leukaemia virus type I and adult T-cell
583 leukaemia-lymphoma. *Lancet Oncol* **15**, e517-526 (2014).
584
585 7. Yasunaga J, Matsuoka M. Molecular mechanisms of HTLV-1 infection and
586 pathogenesis. *Int J Hematol* **94**, 435-442 (2011).
587
588 8. Satou Y, Yasunaga J, Yoshida M, Matsuoka M. HTLV-I basic leucine zipper
589 factor gene mRNA supports proliferation of adult T cell leukemia cells. *Proc*
590 *Natl Acad Sci U S A* **103**, 720-725 (2006).
591
592 9. Miyazaki M, Yasunaga J, Taniguchi Y, Tamiya S, Nakahata T, Matsuoka M.
593 Preferential selection of human T-cell leukemia virus type 1 provirus lacking
594 the 5' long terminal repeat during oncogenesis. *J Virol* **81**, 5714-5723 (2007).
595
596 10. Arnold J, Zimmerman B, Li M, Lairmore MD, Green PL. Human T-cell
597 leukemia virus type-1 antisense-encoded gene, Hbz, promotes T-lymphocyte
598 proliferation. *Blood* **112**, 3788-3797 (2008).
599
600 11. Satou Y*, et al.* HTLV-1 bZIP factor induces T-cell lymphoma and systemic
601 inflammation in vivo. *PLoS Pathog* **7**, e1001274 (2011).
602
603 12. Zhao T*, et al.* HTLV-1 bZIP factor enhances TGF-beta signaling through p300
604 coactivator. *Blood* **118**, 1865-1876 (2011).
605
606 13. Shichijo T*, et al.* Vulnerability to APOBEC3G linked to the pathogenicity of

607 deltaretroviruses. *Proc Natl Acad Sci U S A* **121**, e2309925121 (2024).
608
609 14. Zhao T, *et al.* Human T-cell leukemia virus type 1 bZIP factor selectively
610 suppresses the classical pathway of NF-kappaB. *Blood* **113**, 2755-2764 (2009).
611
612 15. Kinosada H, *et al.* HTLV-1 bZIP Factor Enhances T-Cell Proliferation by
613 Impeding the Suppressive Signaling of Co-inhibitory Receptors. *PLoS Pathog*
614 **13**, e1006120 (2017).
615
616 16. Forlani G, *et al.* Dual cytoplasmic and nuclear localization of HTLV-1-encoded
617 HBZ protein is a unique feature of adult T-cell leukemia. *Haematologica* **106**,
618 2076-2085 (2021).
619
620 17. Forlani G, Baratella M, Tedeschi A, Pique C, Jacobson S, Accolla RS. HTLV-1
621 HBZ Protein Resides Exclusively in the Cytoplasm of Infected Cells in
622 Asymptomatic Carriers and HAM/TSP Patients. *Front Microbiol* **10**, 819 (2019).
623
624 18. Hivin P, *et al.* Nuclear localization of HTLV-I bZIP factor (HBZ) is mediated
625 by three distinct motifs. *J Cell Sci* **118**, 1355-1362 (2005).
626
627 19. Mukai R, Ohshima T. HTLV-1 HBZ positively regulates the mTOR signaling
628 pathway via inhibition of GADD34 activity in the cytoplasm. *Oncogene* **33**,
629 2317-2328 (2014).
630
631 20. Maeda M, *et al.* IL-2/IL-2 Receptor Pathway Plays a Crucial Role in the Growth
632 and Malignant Transformation of HTLV-1-Infected T Cells to Develop Adult T-
633 Cell Leukemia. *Front Microbiol* **11**, 356 (2020).
634
635 21. Usui T, *et al.* Characteristic expression of HTLV-1 basic zipper factor (HBZ)
636 transcripts in HTLV-1 provirus-positive cells. *Retrovirology* **5**, 34 (2008).
637
638 22. Mahgoub M, *et al.* Sporadic on/off switching of HTLV-1 Tax expression is
639 crucial to maintain the whole population of virus-induced leukemic cells. *Proc*
640 *Natl Acad Sci U S A* **115**, E1269-E1278 (2018).
641
642 23. Shen X, Hu PP, Liberati NT, Datto MB, Frederick JP, Wang XF. TGF-beta-
643 induced phosphorylation of Smad3 regulates its interaction with coactivator
644 p300/CREB-binding protein. *Mol Biol Cell* **9**, 3309-3319 (1998).
645
646 24. Ren FJ, Cai XY, Yao Y, Fang GY. JunB: a paradigm for Jun family in immune
647 response and cancer. *Front Cell Infect Microbiol* **13**, 1222265 (2023).
648
649 25. Basbous J, Arpin C, Gaudray G, Piechaczyk M, Devaux C, Mesnard JM. The
650 HBZ factor of human T-cell leukemia virus type I dimerizes with transcription

factors JunB and c-Jun and modulates their transcriptional activity. *J Biol Chem* **278**, 43620-43627 (2003).

26. Tecalco-Cruz AC, Rios-Lopez DG, Vazquez-Victorio G, Rosales-Alvarez RE, Macias-Silva M. Transcriptional cofactors Ski and SnoN are major regulators of the TGF-beta/Smad signaling pathway in health and disease. *Signal Transduct Target Ther* **3**, 15 (2018).

27. Yan X, Liu Z, Chen Y. Regulation of TGF-beta signaling by Smad7. *Acta Biochim Biophys Sin (Shanghai)* **41**, 263-272 (2009).

28. Matsumoto J, Ohshima T, Isono O, Shimotohno K. HTLV-1 HBZ suppresses AP-1 activity by impairing both the DNA-binding ability and the stability of c-Jun protein. *Oncogene* **24**, 1001-1010 (2005).

29. Thebault S, Basbous J, Hivin P, Devaux C, Mesnard JM. HBZ interacts with JunD and stimulates its transcriptional activity. *FEBS Lett* **562**, 165-170 (2004).

30. Nakagawa M*, et al.* Targeting the HTLV-I-Regulated BATF3/IRF4 Transcriptional Network in Adult T Cell Leukemia/Lymphoma. *Cancer Cell* **34**, 286-297 e210 (2018).

31. Ishio T*, et al.* Genome-wide CRISPR screen identifies CDK6 as a therapeutic target in adult T-cell leukemia/lymphoma. *Blood* **139**, 1541-1556 (2022).

32. Hsieh T*, et al.* JunB Is Critical for Survival of T Helper Cells. *Front Immunol* **13**, 901030 (2022).

33. Yamamoto-Taguchi N*, et al.* HTLV-1 bZIP factor induces inflammation through labile Foxp3 expression. *PLoS Pathog* **9**, e1003630 (2013).

34. Zhou L*, et al.* TGF-beta-induced Foxp3 inhibits T(H)17 cell differentiation by antagonizing RORgammat function. *Nature* **453**, 236-240 (2008).

35. Koizumi SI*, et al.* JunB regulates homeostasis and suppressive functions of effector regulatory T cells. *Nat Commun* **9**, 5344 (2018).

36. Katagiri T*, et al.* JunB plays a crucial role in development of regulatory T cells by promoting IL-2 signaling. *Mucosal Immunol* **12**, 1104-1117 (2019).

37. Tanaka-Nakanishi A, Yasunaga J, Takai K, Matsuoka M. HTLV-1 bZIP factor suppresses apoptosis by attenuating the function of FoxO3a and altering its localization. *Cancer Res* **74**, 188-200 (2014).

38. Sundqvist A, *et al.* JUNB governs a feed-forward network of TGFbeta signaling that aggravates breast cancer invasion. *Nucleic Acids Res* **46**, 1180-1195 (2018).

39. Hartmann L, *et al.* Transcriptional regulators ensuring specific gene expression and decision making at high TGFβ doses. *bioRxiv*, 2024.2004.2023.590740 (2024).

40. Peng Q, *et al.* HPV E6/E7: insights into their regulatory role and mechanism in signaling pathways in HPV-associated tumor. *Cancer Gene Ther* **31**, 9-17 (2024).

41. Rahman R, Gopinath D, Buajeeb W, Poomsawat S, Johnson NW. Potential Role of Epstein-Barr Virus in Oral Potentially Malignant Disorders and Oral Squamous Cell Carcinoma: A Scoping Review. *Viruses* **14**, (2022).

42. Keasler VV, Hodgson AJ, Madden CR, Slagle BL. Hepatitis B virus HBx protein localized to the nucleus restores HBx-deficient virus replication in HepG2 cells and in vivo in hydrodynamically-injected mice. *Virology* **390**, 122-129 (2009).

43. Leupin O, Bontron S, Schaeffer C, Strubin M. Hepatitis B virus X protein stimulates viral genome replication via a DDB1-dependent pathway distinct from that leading to cell death. *J Virol* **79**, 4238-4245 (2005).

44. Wang F, *et al.* Role of hepatitis B virus non-structural protein HBx on HBV replication, interferon signaling, and hepatocarcinogenesis. *Front Microbiol* **14**, 1322892 (2023).

45. Cha MY, Ryu DK, Jung HS, Chang HE, Ryu WS. Stimulation of hepatitis B virus genome replication by HBx is linked to both nuclear and cytoplasmic HBx expression. *J Gen Virol* **90**, 978-986 (2009).

46. Weil R, *et al.* Direct association and nuclear import of the hepatitis B virus X protein with the NF-kappaB inhibitor IkappaBalpha. *Mol Cell Biol* **19**, 6345-6354 (1999).

47. Sitterlin D, Bergametti F, Transy C. UVDDB p127-binding modulates activities and intracellular distribution of hepatitis B virus X protein. *Oncogene* **19**, 4417-4426 (2000).

48. Bolger AM, Lohse M, Usadel B. Trimmomatic: a flexible trimmer for Illumina sequence data. *Bioinformatics* **30**, 2114-2120 (2014).

49. Li B, Dewey CN. RSEM: accurate transcript quantification from RNA-Seq data

with or without a reference genome. *BMC Bioinformatics* **12**, 323 (2011).

50. Robinson MD, McCarthy DJ, Smyth GK. edgeR: a Bioconductor package for differential expression analysis of digital gene expression data. *Bioinformatics* **26**, 139-140 (2010).

51. Subramanian A*, et al.* Gene set enrichment analysis: a knowledge-based approach for interpreting genome-wide expression profiles. *Proc Natl Acad Sci U S A* **102**, 15545-15550 (2005).

52. Kanehisa M, Goto S. KEGG: kyoto encyclopedia of genes and genomes. *Nucleic Acids Res* **28**, 27-30 (2000).

53. Langmead B, Salzberg SL. Fast gapped-read alignment with Bowtie 2. *Nat Methods* **9**, 357-359 (2012).

54. Danecek P*, et al.* Twelve years of SAMtools and BCFtools. *Gigascience* **10**, (2021).

55. Amemiya HM, Kundaje A, Boyle AP. The ENCODE Blacklist: Identification of Problematic Regions of the Genome. *Sci Rep* **9**, 9354 (2019).

56. Zhang Y*, et al.* Model-based analysis of ChIP-Seq (MACS). *Genome Biol* **9**, R137 (2008).

57. Wang Q*, et al.* Exploring Epigenomic Datasets by ChIPseeker. *Curr Protoc* **2**, e585 (2022).

58. Ramirez F*, et al.* deepTools2: a next generation web server for deep-sequencing data analysis. *Nucleic Acids Res* **44**, W160-165 (2016).

Acknowledgements

We thank Miho Matsumoto for technical support, Daisuke Kurotaki for technical advice on bioinformatic analyses, and Linda Kingsbury for proofreading. This study was supported by grants from the Project for Cancer Research And Therapeutic Evolution (P-CREATE) (20cm0106306h0005 to M.M., J.Y.); the Research Program on Emerging and Re-emerging Infectious Diseases of the Japan Agency for Medical Research and Development (AMED), (20fk0108088h0002 and 24fk0108629h0003 to M.M. and J.Y.); the Science and Technology Platform Program for Advanced Biological Medicine, also of AMED (21am0401003h0003 to J.Y.); the Japan Society for the Promotion of Science (JSPS) KAKENHI (19H03689 to M.M., 23H02936 to J.Y. 23K15303 to T.S.); the JSPS Core-to-Core Program A, Advanced Research Networks to M.M., J.Y.; the Center for Metabolic Regulation of Healthy Aging (CMHA) to T.S.; and JST SPRING, Grant Number JPMJSP2127 to W.Z..

Author Contributions:

W.Z. acquired funding for the project, performed almost all of the experiments, (including Duolink PLA, gene expression profile, functional analysis, and cell culture assays), performed bioinformatic analysis and data curation, and wrote the paper. T.S. conceived and supervised the project, acquired funding for the project, performed gene expression profile, data curation and bioinformatic analysis, provided clinical samples, and wrote the paper. X.C. provided assistance with the xenograft experiments. M.M. supervised the project, acquired funding for the project, performed data curation. J.Y. conceived and supervised the project, acquired funding for the project, performed data curation, provided clinical samples, and wrote the paper. All authors discussed the results and commented on the manuscript.

Competing interests:

The authors declare that they have no competing interests.

Corresponding authors:

Correspondence to Takafumi Shichijo and Jun-ichirou Yasunaga.

Figure 1

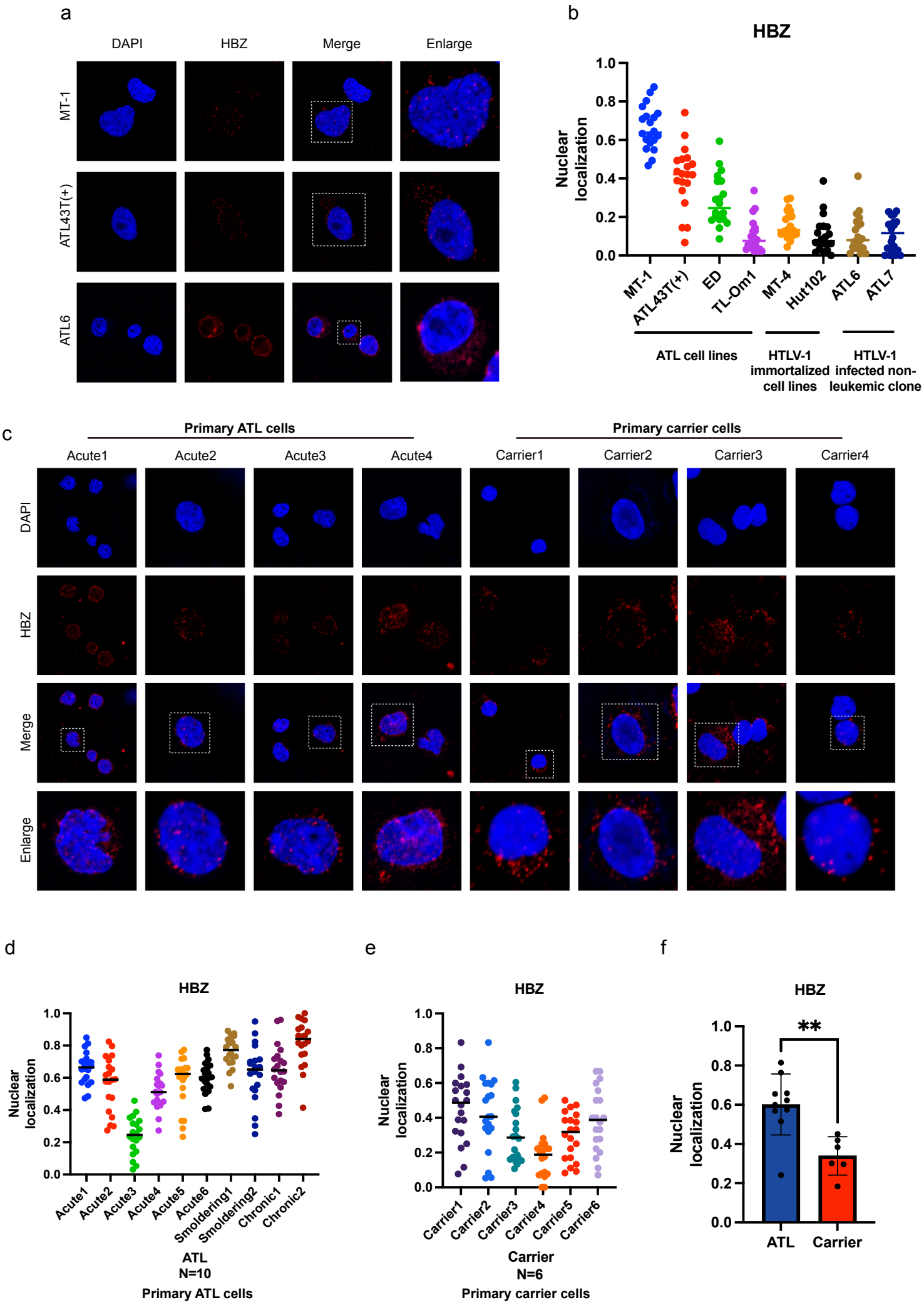
a
DAPI
HBZ
Merge
Enlarge
MT-1
ATL43T(+)
ATL6
b
HBZ
Nuclear localization
1.0
0.8
0.6
0.4
0.2
0.0
MT-1
ATL43T(+)
ED
TL-Om1
MT-4
Hut102
ATL6
ATL7
ATL cell lines
HTLV-1 immortalized cell lines
HTLV-1 infected non-leukemic clone
c
Primary ATL cells
Primary carrier cells
Acute1
Acute2
Acute3
Acute4
Carrier1
Carrier2
Carrier3
Carrier4
DAPI
HBZ
Merge
Enlarge
d
HBZ
Nuclear localization
Acute1
Acute2
Acute3
Acute4
Acute5
Acute6
Smoldering1
Smoldering2
Chronic1
Chronic2
ATL
N=10
Primary ATL cells
e
HBZ
Nuclear localization
Carrier1
Carrier2
Carrier3
Carrier4
Carrier5
Carrier6
Carrier
N=6
Primary carrier cells
f
HBZ
**
Nuclear localization
ATL
Carrier

Fig. 1. Intracellular localization pattern of HBZ protein in various cell lines and patient samples.

a Localization of HBZ protein in MT-1, ATL43T (+) and ATL6 cell lines by Duolink® PLA. **b** The proportion of HBZ that is localized to the nucleus (i.e. nuclear HBZ signals divided by total HBZ signals) is shown for ATL cell lines, HTLV-1 immortalized cell lines and HTLV-1–infected cell lines derived from non-leukemic clones, which were analyzed by ImageJ. 20 randomly selected cells were analyzed for each cell line. **c** Localization of HBZ protein in primary cells from ATL patients (n = 4) and HTLV-1–infected carriers (n = 4) by Duolink® PLA. **d, e** The proportion of HBZ that is localized to the nucleus in each ATL patient sample (n = 10) and HTLV-1–infected carrier sample (n = 6) was analyzed by ImageJ. 20 randomly selected cells were analyzed for each patient. **f** The proportion of HBZ that is localized to the nucleus was compared between ATL (N = 10) and HTLV-1–infected carrier (N = 6) samples (two-tailed unpaired Student's t test; $^{**}P < 0.01$). All experiments were performed at least twice.

Figure 2

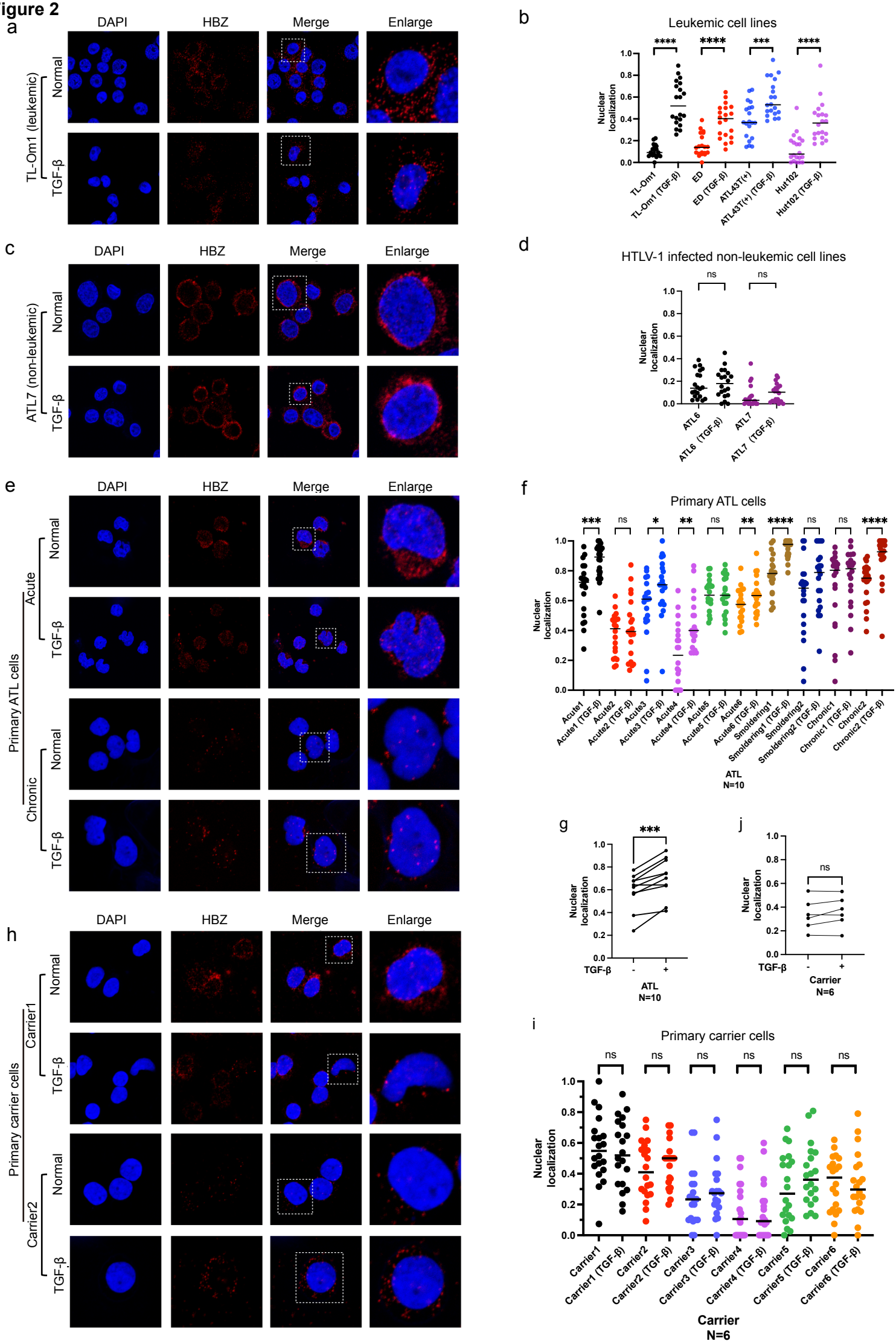
a
DAPI
HBZ
Merge
Enlarge
TL-Om1 (leukemic)
Normal
TGF-β
b
Leukemic cell lines
Nuclear localization
TL-Om1
TL-Om1 (TGF-β)
ED
ED (TGF-β)
ATL43T(+)
ATL43T(+) (TGF-β)
Hut102
Hut102 (TGF-β)
c
ATL7 (non-leukemic)
d
HTLV-1 infected non-leukemic cell lines
ns
ATL6
ATL6 (TGF-β)
ATL7
ATL7 (TGF-β)
e
Primary ATL cells
Acute
Chronic
f
Primary ATL cells
Acute1
Acute1 (TGF-β)
Acute2
Acute2 (TGF-β)
Acute3
Acute3 (TGF-β)
Acute4
Acute4 (TGF-β)
Acute5
Acute5 (TGF-β)
Acute6
Acute6 (TGF-β)
Smoldering1
Smoldering1 (TGF-β)
Smoldering2
Smoldering2 (TGF-β)
Chronic1
Chronic1 (TGF-β)
Chronic2
Chronic2 (TGF-β)
ATL
N=10
g
TGF-β
ATL
N=10
j
Carrier
N=6
h
Primary carrier cells
Carrier1
Carrier2
i
Primary carrier cells
Carrier1
Carrier1 (TGF-β)
Carrier2
Carrier2 (TGF-β)
Carrier3
Carrier3 (TGF-β)
Carrier4
Carrier4 (TGF-β)
Carrier5
Carrier5 (TGF-β)
Carrier6
Carrier6 (TGF-β)
Carrier
N=6

Fig. 2. TGF-β treatment induces nuclear translocation of HBZ protein in ATL cell lines and ATL patient samples.

a, c Localization of HBZ protein in TL-Om1(**a**) and ATL7(**c**) cells with or without TGF-β treatment was detected by Duolink® PLA. **b, d** The proportion of HBZ protein that is localized to the nucleus is shown for ATL cell lines and HTLV-1 immortalized cell lines (**b**) and HTLV-1–infected non-leukemic cell lines (ATL6 and ATL7) (**d**) with or without TGF-β treatment, analyzed using ImageJ. 20 randomly selected cells were analyzed for each cell line. **e** Localization of HBZ protein in primary ATL cells of ATL patients with or without TGF-β treatment. **f-g** The proportion of HBZ protein that is localized to the nucleus in primary ATL cells from 10 ATL patients with or without TGF-β treatment was analyzed individually (**f**) and collectively (**g**) using ImageJ. 20 randomly selected cells were analyzed for each sample. **h** Localization of HBZ protein from primary HTLV-1–infected cells of HTLV-1–infected carrier patients with or without TGF-β treatment. **i, j** The proportion of HBZ protein that is localized to the nucleus in primary HTLV-1–infected cells from 6 HTLV-1–infected carrier patients with or without TGF-β treatment was analyzed individually (**i**) and collectively (**j**) using ImageJ. 20 randomly selected cells were analyzed for each sample. Statistical analyses were performed by two-tailed unpaired Student's t test. * $p < 0.05$, ** $p < 0.01$, *** $p < 0.001$, **** $p < 0.0001$, ns. $P>0.05$. All experiments were performed at least twice.

Figure 3

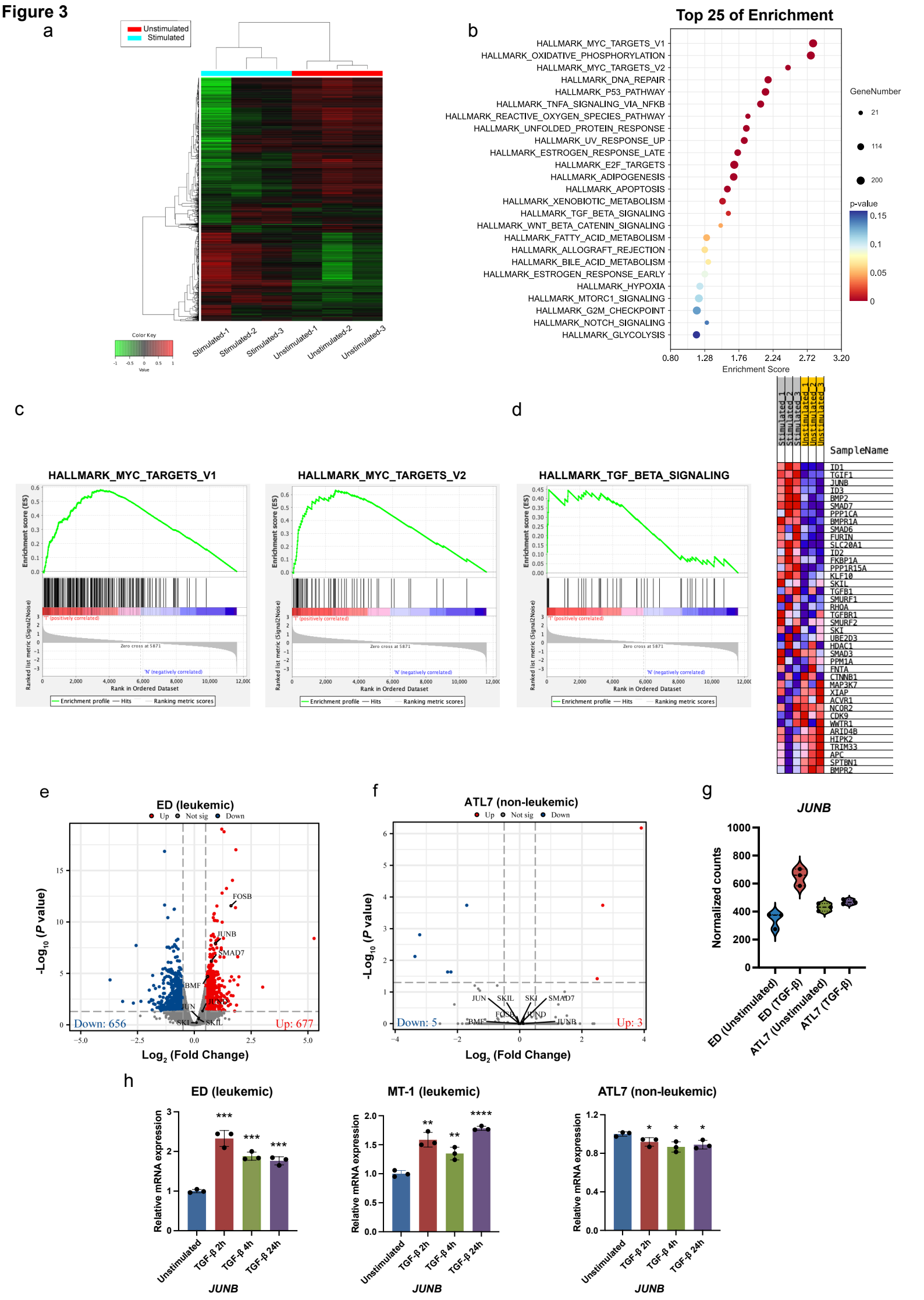
a
Unstimulated
Stimulated
Color Key
Value
Stimulated-1
Stimulated-2
Stimulated-3
Unstimulated-1
Unstimulated-2
Unstimulated-3
b
Top 25 of Enrichment
HALLMARK_MYC_TARGETS_V1
HALLMARK_OXIDATIVE_PHOSPHORYLATION
HALLMARK_MYC_TARGETS_V2
HALLMARK_DNA_REPAIR
HALLMARK_P53_PATHWAY
HALLMARK_TNFA_SIGNALING_VIA_NFKB
HALLMARK_REACTIVE_OXYGEN_SPECIES_PATHWAY
HALLMARK_UNFOLDED_PROTEIN_RESPONSE
HALLMARK_UV_RESPONSE_UP
HALLMARK_ESTROGEN_RESPONSE_LATE
HALLMARK_E2F_TARGETS
HALLMARK_ADIPOGENESIS
HALLMARK_APOPTOSIS
HALLMARK_XENOBIOTIC_METABOLISM
HALLMARK_TGF_BETA_SIGNALING
HALLMARK_WNT_BETA_CATENIN_SIGNALING
HALLMARK_FATTY_ACID_METABOLISM
HALLMARK_ALLOGRAFT_REJECTION
HALLMARK_BILE_ACID_METABOLISM
HALLMARK_ESTROGEN_RESPONSE_EARLY
HALLMARK_HYPOXIA
HALLMARK_MTORC1_SIGNALING
HALLMARK_G2M_CHECKPOINT
HALLMARK_NOTCH_SIGNALING
HALLMARK_GLYCOLYSIS
0.80
1.28
1.76
2.24
2.72
3.20
Enrichment Score
GeneNumber
21
114
200
p-value
0.15
0.1
0.05
0
c
HALLMARK_MYC_TARGETS_V1
HALLMARK_MYC_TARGETS_V2
HALLMARK_TGF_BETA_SIGNALING
Enrichment score (ES)
Ranked list metric (Signal2Noise)
'T' (positively correlated)
Zero cross at 5871
'N' (negatively correlated)
Rank in Ordered Dataset
Enrichment profile
Hits
Ranking metric scores
d
Stimulated_1
Stimulated_2
Stimulated_3
Unstimulated_1
Unstimulated_2
Unstimulated_3
SampleName
ID1
TGIF1
JUNB
ID3
BMP2
SMAD7
PPP1CA
BMPR1A
SMAD6
FURIN
SLC20A1
ID2
FKBP1A
PPP1R15A
KLF10
SKIL
TGFB1
SMURF1
RHOA
TGFBR1
SMURF2
SKI
UBE2D3
HDAC1
SMAD3
PPM1A
FNTA
CTNNB1
MAP3K7
XIAP
ACVR1
NCOR2
CDK9
WWTR1
ARID4B
HIPK2
TRIM33
APC
SPTBN1
BMPR2
e
ED (leukemic)
Up
Not sig
Down
-Log10 (P value)
Log2 (Fold Change)
FOSB
JUNB
SMAD7
BMF
JUN
FOSB
SKI
SKIL
Down: 656
Up: 677
f
ATL7 (non-leukemic)
Up
Not sig
Down
-Log10 (P value)
Log2 (Fold Change)
JUN
SKIL
SKI
SMAD7
FOSB
JUND
BMF
JUNB
Down: 5
Up: 3
g
JUNB
Normalized counts
ED (Unstimulated)
ED (TGF-β)
ATL7 (Unstimulated)
ATL7 (TGF-β)
h
ED (leukemic)
MT-1 (leukemic)
ATL7 (non-leukemic)
Relative mRNA expression
Unstimulated
TGF-β 2h
TGF-β 4h
TGF-β 24h
JUNB

Fig. 3. TGF-β-dependent transcriptional regulation in the ED cell line.

ED cells were subjected to RNA-seq with or without 2-hour TGF-β treatment. **a** Heatmap of relative mRNA expression levels in TGF-β stimulated ED cells vs. unstimulated ED cells. **b** Hallmark gene sets upregulated in ED cells upon TGF-β treatment, analyzed by Gene Set Enrichment Analysis (GSEA). **c** Myc-associated gene signatures are significantly enriched in TGF-β stimulated ED cells compared with unstimulated ED cells, as determined by GSEA with RNA-seq. **d** Significantly enriched gene signatures for the TGF-β related gene set (left) and enriched genes (right) were determined by GSEA. **e** Volcano plot representing genes differentially expressed in TGF-β stimulated ED cells vs. unstimulated cells. Genes considered significantly upregulated or downregulated are highlighted in red and blue, respectively. Genes with insignificant changes are highlighted in grey. **f** Volcano plot representing genes differentially expressed in TGF-β treated ATL7 cells vs. unstimulated cells. **g** Normalized counts of *JUNB* in TGF-β treated ED cells and ATL7 cells vs. control cells. **h** *JUNB* mRNA levels in ED, MT-1 and ATL7 cell lines without or with TGF-β treatment for 2, 4 or 24 hours were analyzed by RT-qPCR (triplicate experiments, * $p < 0.05$, ** $p < 0.01$, *** $p < 0.001$, **** $p < 0.0001$).

Figure 4

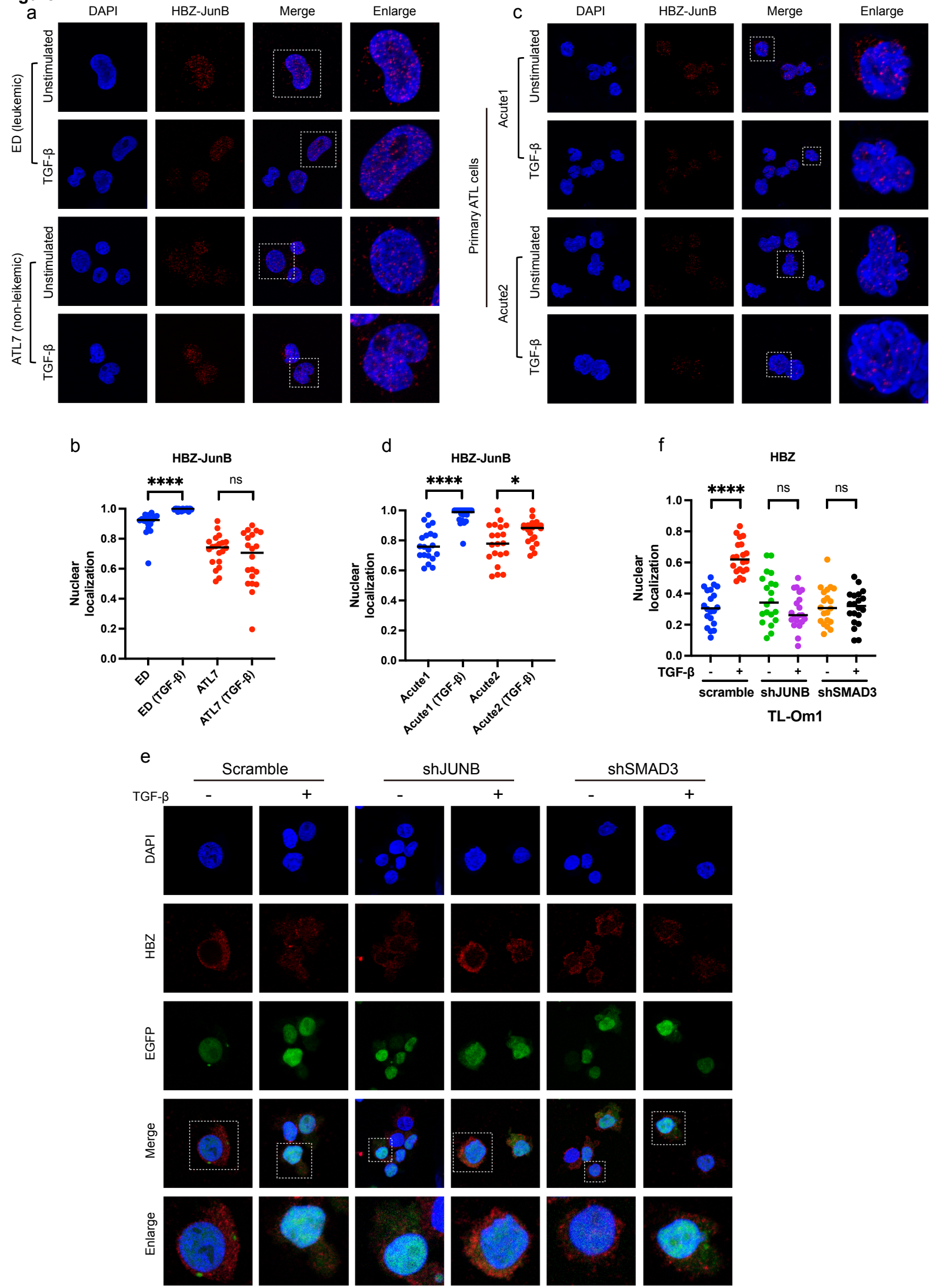
a
DAPI
HBZ-JunB
Merge
Enlarge
ED (leukemic)
Unstimulated
TGF-β
ATL7 (non-leikemic)
Unstimulated
TGF-β
c
DAPI
HBZ-JunB
Merge
Enlarge
Primary ATL cells
Acute1
Unstimulated
TGF-β
Acute2
Unstimulated
TGF-β
b
HBZ-JunB
****
ns
Nuclear localization
1.0
0.8
0.6
0.4
0.2
0.0
ED
ED (TGF-β)
ATL7
ATL7 (TGF-β)
d
HBZ-JunB
****
*
Nuclear localization
1.0
0.8
0.6
0.4
0.2
0.0
Acute1
Acute1 (TGF-β)
Acute2
Acute2 (TGF-β)
f
HBZ
****
ns
ns
Nuclear localization
1.0
0.8
0.6
0.4
0.2
0.0
TGF-β
-
+
-
+
-
+
scramble
shJUNB
shSMAD3
TL-Om1
e
Scramble
shJUNB
shSMAD3
TGF-β
-
+
-
+
-
+
DAPI
HBZ
EGFP
Merge
Enlarge

Fig. 4. JunB plays a role in the translocation of HBZ to the nucleus induced by TGF-β treatment.

a Complexes of JunB with HBZ in ED and ATL7 cell lines with or without TGF-β treatment were detected by Duolink® PLA. **b** The proportion of HBZ-JunB complexes that are localized to the nucleus in TGF- β treated and untreated ED and ATL7 cell lines was analyzed by ImageJ. 20 randomly selected cells were analyzed for each cell line. **c** HBZ-JunB complexes in primary ATL cells of ATL patients with acute-type with or without TGF-β treatment were detected by Duolink® PLA. **d** The proportion of HBZ-JunB complexes that are localized to the nucleus in primary ATL cells of acute-type ATL patients with or without TGF-β stimulation was analyzed by ImageJ. 20 randomly selected cells were analyzed for each sample. **e** Localization of HBZ in TL-Om1 cells infected with scramble shRNA, shJUNB or shSMAD3 lentivirus vectors, with or without TGF-β stimulation. **f** The proportion of HBZ protein that is localized to the nucleus in (**e**) was analyzed by ImageJ. 20 randomly selected cells were analyzed for each sample. Statistical analyses were performed by two-tailed unpaired Student's t test. * $p < 0.05$, **** $p < 0.0001$, ns. $p > 0.05$. All experiments were performed at least twice.

Figure 5

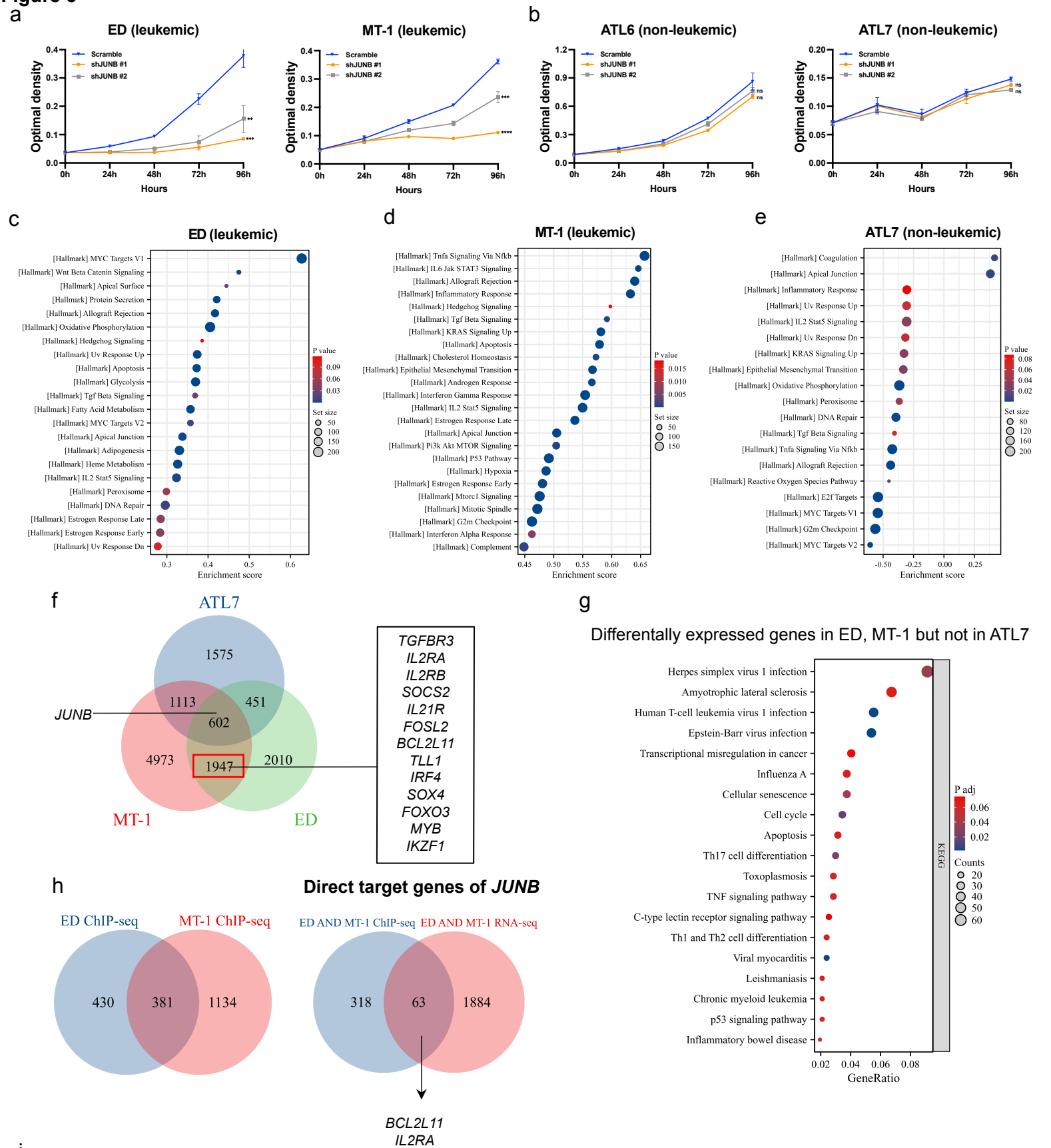

Enrichment in:	ED shJUNB-TGFβ2h VS ED shJUNB-unstimulated			ED TGFβ2h VS Unstimulated (Significant enrichment in Fig.3B)		
HALLMARK GS DETAILS	NES	NOM p-val	FDR q-val	NES	NOM p-val	FDR q-val
MYC_TARGETS_V1	1.11	0.214	0.436	2.80	0.000	0.000
OXIDATIVE_PHOSPHORYLATION	1.16	0.146	0.397	2.77	0.000	0.000
MYC_TARGETS_V2	1.30	0.087	0.208	2.45	0.000	0.000
DNA_REPAIR	0.73	0.983	0.949	2.17	0.000	0.000
P53_PATHWAY	1.12	0.229	0.434	2.13	0.000	0.000
TNFA_SIGNALING_VIA_NFKB	1.51	0.008	0.075	2.06	0.000	0.000
REACTIVE_OXYGEN_SPECIES_ PATHWAY	1.55	0.011	0.099	1.89	0.000	0.001
UV_RESPONSE_UP	1.32	0.045	0.197	1.84	0.000	0.001
ESTROGEN_RESPONSE_LATE	1.41	0.015	0.122	1.74	0.000	0.005
E2F_TARGETS	0.78	0.962	0.979	1.69	0.000	0.006
TGF_BETA_SIGNALING	1.83	0.000	0.014	1.61	0.013	0.014
APOPTOSIS	0.90	0.683	0.798	1.60	0.000	0.014

Fig. 5. JunB-dependent transcriptional regulation in ATL cells.

a Cell growth of ED (left) and MT-1 (right) cells infected with shJUNB#1 or shJUNB#2 (normalized mean ± s.d. of triplicate experiments). **b** Cell growth of ATL6 (left) and ATL7 (right) cells infected with shJUNB#1 or shJUNB#2 (normalized mean ± s.d. of triplicate experiments). **c-e** Significantly enriched gene signatures in *JUNB* knockdown cells, determined by Gene Set Enrichment Analysis (GSEA) with RNA-seq in ED (**c**), MT-1 (**d**) and ATL7 (**e**) cells. **f** Venn diagram showing the overlap of differentially expressed genes identified in *JUNB* knockdown cells vs, control cells in ED, MT-1 and ATL7 cells. **g** Kyoto Encyclopedia of Genes and Genomes (KEGG) analysis of genes that are found to be differentially expressed (*JUNB* knockdown cells vs. control cells) in ED and MT-1 but not ATL7 cells. **h** Venn diagram showing the overlap of JunB target genes (by ChIP-seq) and genes found by RNA-seq to be differentially expressed in both ED and MT-1 cells, but not in ATL7 cells. **i** Volcano plot (left) showing genes differentially expressed in TGF-β stimulated *JUNB* knockdown ED cells compared with unstimulated knockdown cells. Genes considered significantly upregulated or downregulated are highlighted in red and blue, respectively. Genes with insignificant changes are highlighted in grey. The table (right) shows the GSEA of gene expression after TGF-β stimulation for *JUNB* knockdown cells and parental ED cells. Gene sets are significantly enriched at FDR < 0.05.

Figure 6

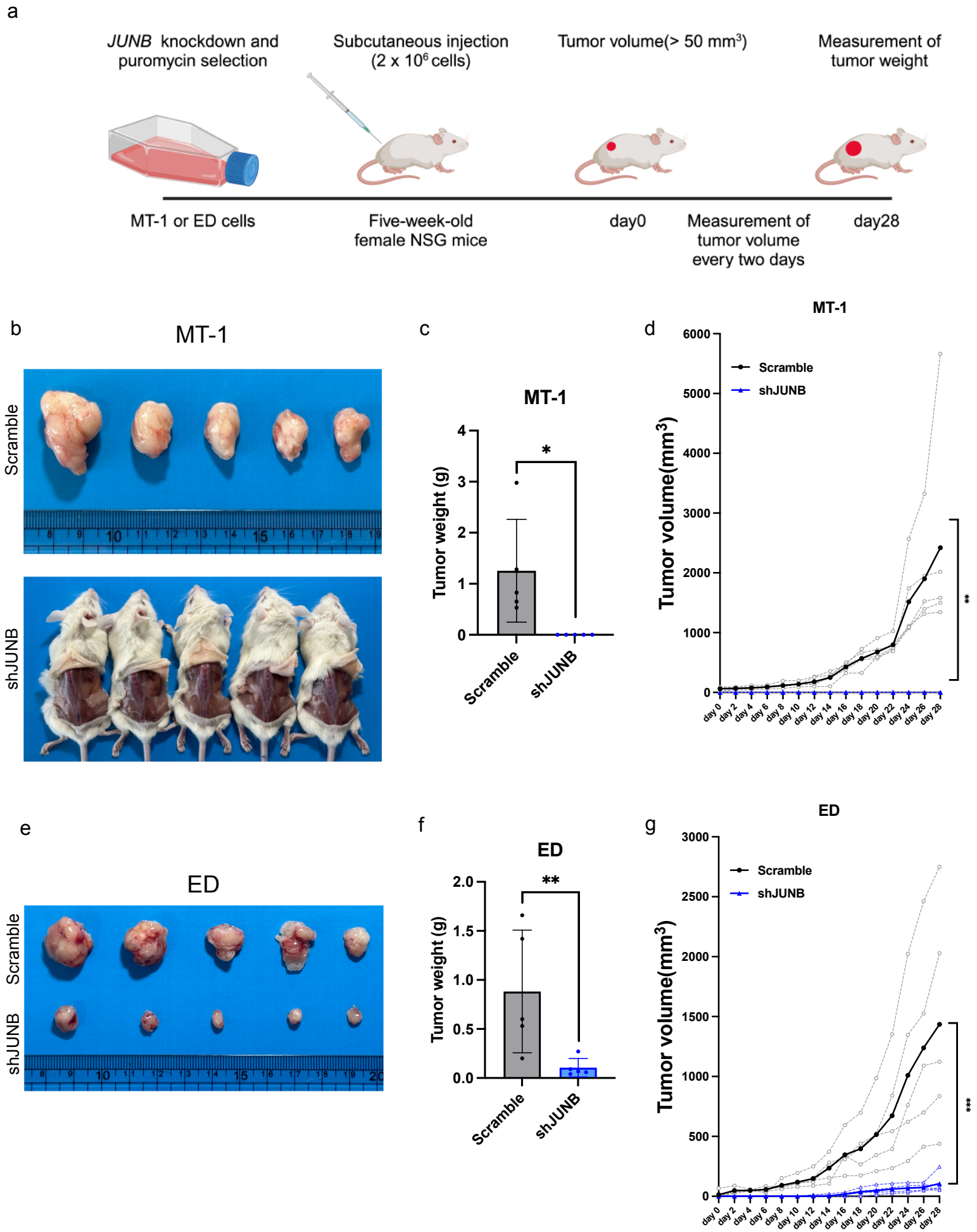
a
JUNB knockdown and puromycin selection
Subcutaneous injection (2 x 10^6 cells)
Tumor volume(> 50 mm^3)
Measurement of tumor weight
MT-1 or ED cells
Five-week-old female NSG mice
day0
Measurement of tumor volume every two days
day28
b
MT-1
Scramble
shJUNB
c
MT-1
Tumor weight (g)
Scramble
shJUNB
d
MT-1
Scramble
shJUNB
Tumor volume(mm^3)
e
ED
Scramble
shJUNB
f
ED
Tumor weight (g)
Scramble
shJUNB
g
ED
Scramble
shJUNB
Tumor volume(mm^3)

Fig. 6. JunB depletion leads to ATL tumor growth inhibition *in vivo*.

a Schematic representation of the xenograft model of ATL. **b** ATL tumor growth in mice subcutaneously injected with scramble shRNA (n = 5) or shJUNB (n = 5) infected MT-1 cells. **c, d** ATL tumor weights (normalized mean ± s.d) (**c**) and volumes (**d**) in the mice subcutaneously injected with scramble shRNA (n = 5) or shJUNB (n = 5) infected MT-1 cells. **e** ATL tumor growth in mice subcutaneously injected with scramble shRNA (n = 5) or shJUNB (n = 5) infected ED cells. **f, g** ATL tumor weights (normalized mean ± s.d) (**f**) and volumes (**g**) in the mice subcutaneously injected with scramble shRNA (n = 5) or shJUNB (n = 5) infected ED cells. Statistical analysis is by two-tailed unpaired Student's t test; * $p < 0.05$, ** $p < 0.01$, *** $p < 0.001$).